World Academy of Science, Engineering and Technology
International Journal of Biotechnology and Bioengineering
Vol:14, No:9, 2020

# Corrosion Study of Magnetically Driven Components in Spinal Implants by Immersion Testing in Simulated Body Fluids

Benjawan Saengwichian, Alasdair E. Charles, Philip J. Hyde



***Abstract*—**Magnetically controlled growing rods (MCGRs) have been used to stabilise and correct spinal curvature in children to support non-invasive scoliosis adjustment. Although the encapsulated driving components are intended to be isolated from body fluid contact, *in vivo* corrosion was observed on these components due to sealing mechanism damage. Consequently, a corrosion circuit is created with the body fluids, resulting in malfunction of the lengthening mechanism. Particularly, the chloride ions in blood plasma or cerebrospinal fluid (CSF) may corrode the MCGR alloys, possibly resulting in metal ion release in long-term use. However, there is no data available on the corrosion resistance of spinal implant alloys in CSF. In this study, an *in vitro* immersion configuration was designed to simulate *in vivo* corrosion of 440C SS-Ti6Al4V couples. The 440C stainless steel (SS) was heat-treated to investigate the effect of tempering temperature on intergranular corrosion (IGC), while crevice and galvanic corrosion were studied by limiting the clearance of dissimilar couples. Tests were carried out in a neutral artificial cerebrospinal fluid (ACSF) and phosphate-buffered saline (PBS) under aeration and deaeration for 2 months. The composition of the passive films and metal ion release were analysed. The effect of galvanic coupling, pH, dissolved oxygen and anion species on corrosion rates and corrosion mechanisms are discussed based on quantitative and qualitative measurements. The results suggest that ACSF is more aggressive than PBS due to the combination of aggressive chlorides and sulphate anions, while phosphate in PBS acts as an inhibitor to delay corrosion. The presence of Vivianite on the SS surface in PBS lowered the corrosion rate (CR) more than 5 times for aeration and nearly 2 times for deaeration, compared with ACSF. The CR of 440C is dependent on passive film properties varied by tempering temperature and anion species. Although the CR of Ti6Al4V is insignificant, it tends to release more Ti ions in deaerated ACSF than under aeration, about 6 µg/L. It seems the crevice-like design has more effect on macroscopic corrosion than combining the dissimilar couple, whereas IGC is dominantly observed on sensitized microstructure.

***Keywords*—**Cerebrospinal fluid, crevice corrosion, intergranular corrosion, magnetically controlled growing rods.

## I. Introduction

THE application of bio-implant alloys, for instance, 316L SS, titanium alloy (Ti), cobalt chrome alloy (CoCr) and nitinol (Ti-Ni) are all promising choices for orthopaedic implants [1]. For serving reconstructive and arthroplasty surgeries, the combination of dissimilar alloys such as SS-Ti, Ti-CoCr or SS-CoCr have been applied to achieve the unique functionality. Recently, to support non-invasive treatment, encapsulated magnetic implants have been developed [2]-[4]. The non-implant grade alloys and titanium coated magnet have been designed and used as the internal parts with the purpose of dry and non-invasive use. For example, MCGRs have been widely used for early-onset scoliosis treatment as illustrated in Fig. 1 (a). Every typical 3-6 months, the MCGR is non-invasively extended by using an external magnetic controller to spin the internal magnet of the MCGR as presented in Fig. 1 (b).

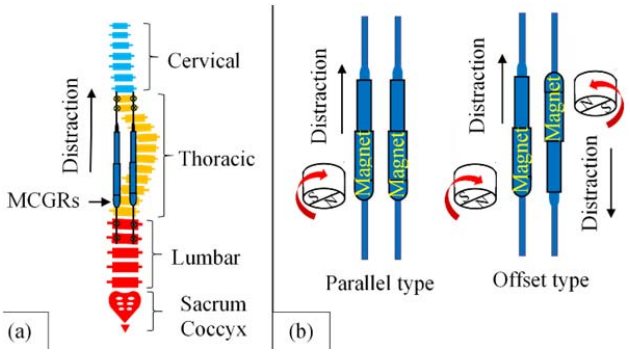


Fig. 1 (a) A schematic of the spinal curvature disorder (scoliosis) implanted with MCGRs, and (b) MCGR types with external magnetic controllers.

The MCGR is extended by the screw driving components including a Ti coated magnet, a 440C SS drive pin and ball bearing, and a Ti6Al4V leadscrew and rod as presented in Fig. 2 (a). These dissimilar components are encapsulated by a Ti6Al4V casing and an O-ring seal. When the internal magnet is remotely spun, the drive pin will turn the leadscrew and then the rod is lengthened (distraction) as in Fig. 2 (b). Eventually, the spine curvature is gradually corrected.

Recently, some studies have reported the premature failure of MCGRs related to the combination of wear and corrosion in the casing [5], [6] and the presence of metallosis [7]. We believe that there is a possibility of sealing mechanism leaks which allows body fluids to contact with the screw driving components inside the casing. As body fluid contains electrolytes for maintaining metabolism system such as dissolved salts of bicarbonates ($HCO_3^-$), chlorides ($Cl^-$) and sulphates ($SO_4^{2-}$) ions, implant alloys undergo corrosion during long-term exposure [8]. The mode of corrosion and its

B. Saengwichian and A. E. Charles are with the School of Engineering, Newcastle University, Newcastle upon Tyne, NE1 7RU, UK (e-mail: b.saengwichian2@newcastle.ac.uk, alasdair.charles@newcastle.ac.uk).

P. J. Hyde is with the School of Engineering, Newcastle University, Newcastle upon Tyne, NE1 7RU, UK (corresponding author, phone: 0191 20 86196; e-mail: philip.hyde@newcastle.ac.uk).

severity depends on pH, the concentration of anion species and dissolved oxygen (DO) level of the implant environment.

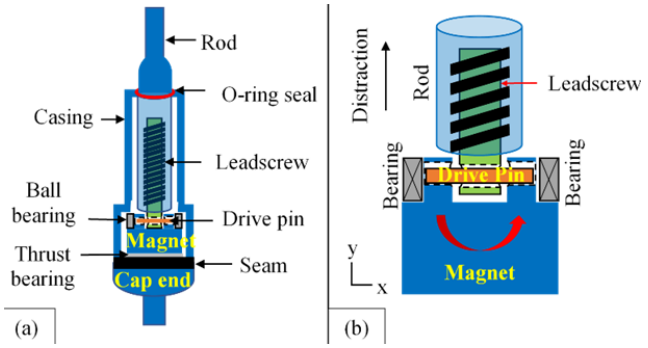


Fig. 2 (a) A schematic of MCGR components, and (b) the encapsulated driving components

Data from the British Association of Spine Surgeons across 14 institutions indicated the common complications of dural tears during spinal operation up to 25% [9]. Some patients underwent the delayed symptoms of CSF leakage and postoperative infection after spinal implantation [10]-[18]. It has been reported that pH of body fluid could be changed from the normal value at 7.4 to localized pH at 5.5 (acid) or 9 (alkaline) in the presence of infections at the surgical site [19]. The variations of local pH could result in severe localized corrosion of alloy implants [8]. Comparing to blood plasma, CSF contains 20% higher $Cl^-$ ions and little protein, less than 0.5 mmol/L [20]. In terms of DO level, it is varied by the partial pressure of oxygen ($P_{O2}$) in body fluids. The $P_{O2}$ in arterial and venous blood varies between 100 and 40 mmHg, respectively, whereas that of CSF is about 25-53 mmHg. The DO in arterial blood without hemoglobin combination is about 4.5 ppm, whereas that of venous blood is about 1.8 ppm. In CSF, DO varies between 1.1-2.4 ppm. Since $P_{O2}$ *in vivo* varies, there is a possibility of implant surface producing differential aeration cells [8].

A 440C martensitic SS contains 17 wt.%Cr and 1 wt.%C, it is widely used for making surgical cutting tools (non-implant grade) as it can be hardened by heat treatment (HT) [1]. Comparing with the implant grade alloys like 316L SS having similar Cr contents, a tempered 440C SS has superior wear resistance and magnetic properties, but corrosion resistance is lower. Also, it tends to be sensitized due to chromium depletion at the vicinity of grain boundaries (GBs) if it is heat-treated at the critical temperature range of 450 – 600 °C, and consequently is much more susceptible to IGC and cracking in chloride environment [21], [22]. Bonagani et al. indicate that the maximum degree of sensitization was observed at 550 °C tempering, while uniform corrosion was revealed at tempering temperature below 400 °C [23]. The authors also reported deficiency of pitting corrosion resistance was observed at the critical temperature range [24]. Additionally, the combination of dissimilar coupling design on galvanic corrosion *in vivo* is still unclear [25]. Especially, the application of 440C SS-Ti6Al4V coupling *in vivo* is nascent, and corrosion data in the different physiological environment are unavailable.

In our work, the construct of screw driving components in an MCGR casing [Fig. 2 (b)] has been simulated by using a 440C SS-Ti6Al4V coupling of similar design but larger scale [Fig. 3 (a)]. The *in vitro* immersion test was designed to evaluate and compare corrosion resistance of both unsensitized and sensitized 440C SS, as well as obtain insight of *in vivo* corrosion mechanism of those dissimilar couples. Tests were conducted in 37 °C ACSF and PBS under aeration (5 ppm) and deaeration (1 ppm) for 2 months. CRs based on mass loss were determined for evaluation. The passive films and metal ion release were characterized. The factors affecting CRs were then discussed based on the quantitative and qualitative measurements.

## II. Materials and Methods

### A. Alloys

A medical-grade 440C martensitic stainless steel (MSS) and Ti6Al4V Eli grade 23 round bars according to ASTM F899-12b [26] and ASTM F136-08 [27] standards were selected to mimic the dissimilar couplings of MCGR screw driving components as presented in Fig. 2 (b). The 440C rod represented the drive pin and the Ti6Al4V collars act for the coupling parts, with the dimension scaling up to 12.5 times of the original. The clearance fits between 440C SS rods and Ti6Al4V collars were mimicking that of the retrieved drive pins and the screw driving components, about 100 µm. The dimension of the 440C rod and Ti6Al4V collars is indicated in Fig. 3 (a). The 440C rods were hardened by heating up to 1050 °C for 30 min in an argon shielding furnace, following by water quenching. Then, the rods were tempered at 200 and 550 °C for 2 hours, designated as T200 and T550. The T200 samples attributed unsensitized microstructure, while T550 had sensitized microstructure. After HT, all samples were polished with successively finer silicon carbide (SiC) papers to 1000 grit finish, with the average roughness (Ra) less than 0.2 µm.

The 440C samples coupled with Ti6Al4V collars were set up in a vacuum container as illustrated in Fig. 3 (b). The gaps between Ti6Al4V collars were separated by using a 1 mm acrylic sheet. Before testing, all samples were cleaned with ethanol and an ultrasonic cleaner.

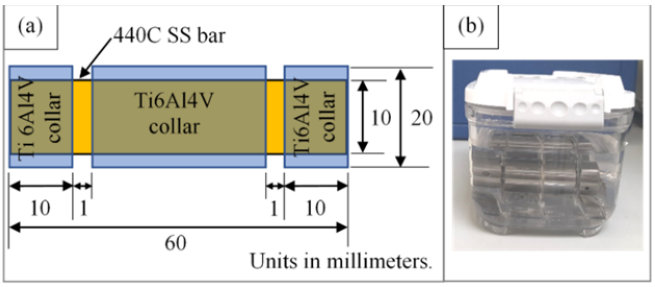


Fig. 3 Schematics of the test configuration. (a) the dimension of 440C rod and Ti6Al4V collars, and (b) a corrosion cell set-up

### B. Physiological Solutions

Biocyte® modified ACSF and Melford® PBS were selected

for the *in vitro* study. Both solutions were un-diluted. The chemical compositions and pH of ACSF and PBS used for this study are given in Table I.

TABLE I
COMPOSITIONS OF ACSF AND PBS IN MMOL/L (MM)

| Compositions | ACSF | PBS |
|---|---|---|
| NaCl | 151 mM | 137 mM |
| KCl | 3 mM | 2.7 mM |
| $CaCl_2 \cdot 2H_2O$ | 2.5 mM | - |
| $Na_2HPO_4$ | - | 10 mM |
| $KH_2PO_4$ | - | 1.9 mM |
| $MgSO_4 \cdot 7H_2O$ | 1.3 mM | - |
| $C_6H_{12}O_6H_2O$ | 13 mM | - |
| HEPES ($C_8H_{18}N_2O_4S$) | 5 mM | - |
| pH | 7.3 - 7.4 | 7.2 - 7.6 |

The ACSF contained corrosive chloride ($Cl^-$) and sulphate ($SO_4^{2-}$) ions, with 5.63 and 0.75 g/L respectively, whereas the PBS included $Cl^-$ ion of 4.95 g/L and phosphate ($PO_4^{3-}$) inhibitor of 1.13 g/L.

### C. In vitro Immersion Test

The immersion test was conducted according to ASTM G31-72(2004): Standard Practice for Laboratory Immersion Corrosion Testing of Metals [28]. There were three different parameters studied including anion species, DO, and unsensitized (T200) and sensitized (T550) microstructures.

The corrosion cells included T200 and T550 rods coupled with Ti6Al4V collars which were immersed in ACSF and PBS under natural aeration (5 ppm) and deaeration (1 ppm) for 2 months. Deionized (DI) water was used for comparison. Under the deaerated condition, the solutions were purged with nitrogen gas for 5 minutes in a vacuum container. The concentration of DO was measured at laboratory room temperature by using a WTW Multi 350i DO meter.

The volume of the corrosion cell as shown in Fig. 3 (b) was 500 ml. The ratio of solution volume to sample surface area (V/S) was in the range of 6-12 mL/cm$^2$. All corrosion cells were maintained at 37 ± 0.2 °C in a VWR IL53 incubator.

The pH and conductivity were measured by using a HANNA pH tester model HI98103 and a radiometer analytical model pIONneer 30, respectively. Two testing conditions including aerated ACSF and PBS were reproducible for checking pH variations.

CR was determined based on (1) according to the ASTM G31. Mass loss was measured by using a KERN analytical balance model ABT220-5DM with an accuracy of 0.5 mg.

$$CR = \frac{K\Delta m}{A\rho t} \quad (1)$$

where K= conversion factor = 87,600 mm/year, $\Delta m$ is the change of mass (mg), A is the original surface area exposed to the corrosive media (cm$^2$), $\rho$ is the density of sample (g/cm$^2$) and t is the exposure time (h).

### D. Surface Morphology Analysis

After the immersion test, the physical change in macroscopic surface morphology of 440C rods was photographed. The microscopic morphology was investigated by using a Hitachi scanning electron microscope (SEM) model TM3030. There were two investigated areas on 440C SS rods including the coupling areas defined as the confined areas, and both gaps between the collars indicated as the exposed areas.

### E. Corrosion Products and Passive Film Characterization

An Energy Dispersive X-Ray (EDX), JEOL JSM-5600LV model, was used to characterize the elemental composition of passive films on 440C rods. Corrosion products were collected from the corrosion cells and dehydrated at 50 °C for 1 hour. An X-Ray Powder Diffraction (XRPD) was used to identify the crystalline phase of powdered corrosion products.

### F. Metal Ion Release Measurement

After 2-month immersion tests, the solutions were filtered with Whatman® 0.4 µm glass microfiber filters and acidified with 1% nitric acid by volume to maintain the interested analytes in solution. An Inductively Coupled Plasma-Optical Emission Spectrometry, ICP-OES Optima 8000 model, was used to measure the concentration of dissolved iron (Fe), titanium (Ti) and chromium (Cr) ions in ACSF and PBS. Before the analysis, the standard iron, chromium and titanium solutions were used for calibration.

## III. RESULTS

### A. In vitro Immersion Test

The first-week immersion, ACSF and DI water changed from clear solutions into brown and turbid. The physical change in PBS began 4 weeks after, turning into pale and turbid. All solutions became darker by the immersion time as the representative images shown in Fig. 4. Some salt sediments were observed in ACSF and PBS as presented in Figs. 4 (a)-(d).

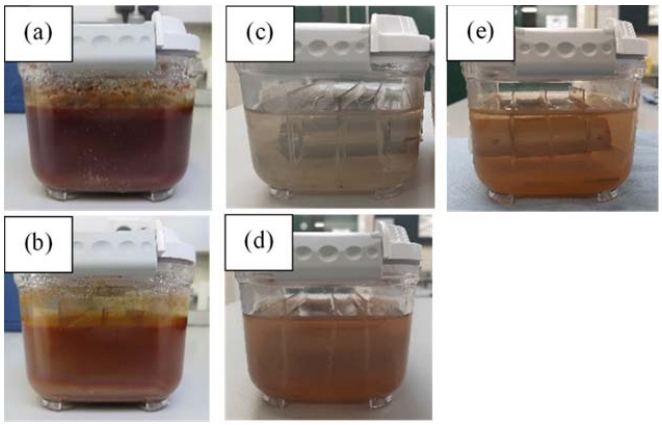


Fig. 4 Physical appearance, after 2-month immersion, of (a) aerated ACSF, (b) deaerated ACSF, (c) aerated PBS, (d) deaerated PBS and (e) aerated deionized water.

Fig. 5 exhibits different trends in pH of all solutions. The pH values of aerated and deaerated ACSF became acidic (5.5-5.6) after 2-month immersion, whereas that of both PBS was

likely to increase (9.7-11.2). The tendency of pH for both solutions reached a plateau after 2 months. The pH values of aerated DI water decreased and fluctuated in the range of 5-6.

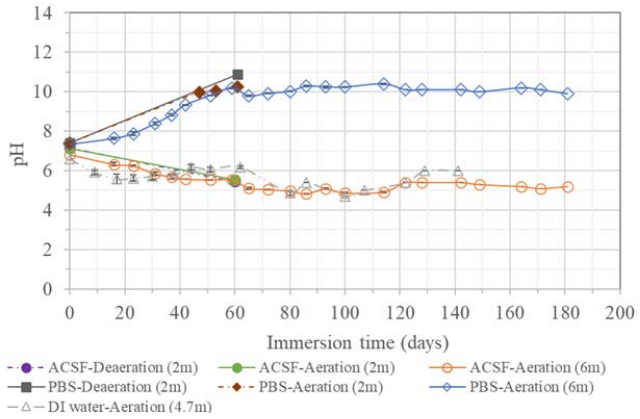


Fig. 5 pH variations by the immersion time

The post-test conductivity after 2-month immersion was significantly increased by 28-30% for ACSF and PBS, as presented in Table II. Regarding the inherent low conductivity of DI water, there was much change from 2.85 to 25.5 µs/cm.

TABLE II
ELECTRICAL CONDUCTIVITY CHANGE IN ms/cm

| Solutions | ACSF | PBS | DIW |
|---|---|---|---|
| Before immersion | 15.0 | 16.7 | 2.85 µs/cm |
| After 2-month immersion | 19.2 | 21.7 | 25.5 µs/cm |

Fig. 6 (a) exhibits the influence of anion species in all solutions on CRs of T200 and T550 rods. The ACSF containing both corrosive $Cl^-$ and $SO_4^{2-}$ ions were more aggressive than others, with CR of 272-478 µm/yr for T200 and 99-320 µm/yr for T550. The tendency of CR in PBS was significantly lower than ACSF, with 92-165 µm/yr for T200 and 183-214 µm/yr for T550 as there was $PO_4^{3-}$ inhibitor with the ratio of $Cl^-/PO_4^{3-}$ = 4.4:1. Additionally, the concentration of $Cl^-$ ions was about 14% lower than ACSF. Despite very low ion concentration, the CR in DI water was in the range of 18-34 µm/yr. In terms of sensitization effect, the comparing CR in ACSF indicated that less corrosion was observed on T500 than T200, about 1.5 times in aeration and 3 times in deaeration. Conversely, T200 had better corrosion resistance than T550 in PBS and DI water, about 2 times lower CR. Considering the effect of DO level in Fig. 6 (b), the CR of both T200 and T550 in aerated ACSF was higher than deaeration, whereas the CR in deaerated PBS became lower than aeration.

### *B. Surface Morphology*

Fig. 7 illustrates the macroscopic surface morphology of T200 and T550 SS rods in ACSF and PBS under aerated and deaerated conditions. Intensive green rust (GR) film was observed in aerated and deaerated PBS and ACSF, preferentially covering at the confined areas of T200 rods as presented in Figs. 7 (a)-(d), whereas partial discoloration (matte appearance) with scattering black rust was observed on T550 rods as in Fig. 7 (e)-(h). Some pits were also observed in the exposed areas of T550 rods between both gaps of collars and propagated to the confined areas. The shiny areas represented the finishing surface or uncorroded areas.

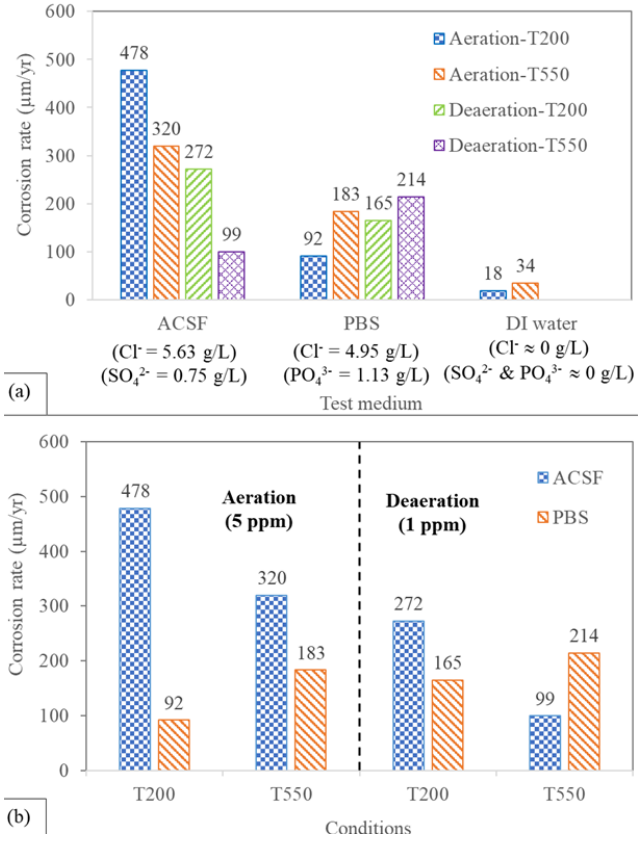


Fig. 6 (a) Influence of anion species and (b) DO level on CRs of T200 and T550 rods.

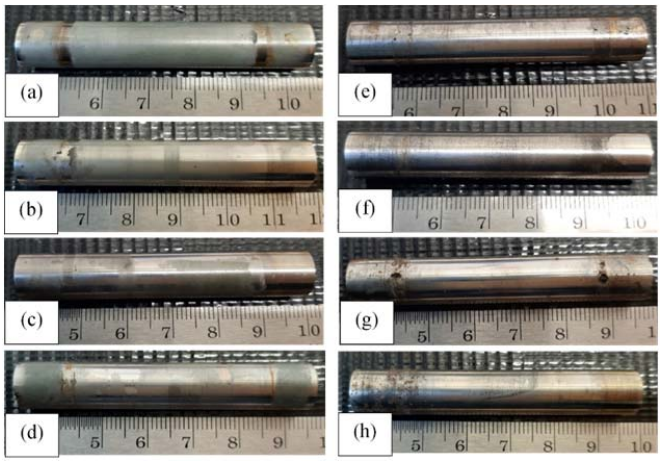


Fig. 7 Macroscopic surface morphology of (a), (b) T200-aerated and deaerated ACSF, (c), (d) T200-aerated and deaerated PBS, (e), (f) T550-aerated and deaerated ACSF, and (g), (h) T550-aerated and deaerated PBS

The microscopic morphology images are given in Fig. 8.

On the GR film of T200 surface, a mud-cracking pattern which resulted from the dehydration process of passive film was mainly observed as presented in Figs. 8 (a), (c), (d). Fig. 8 (b) shows the typical feature of general corrosion after GR film removal. The feature of pit formation on T200 surface did not relate to GB attack as in Fig. 8 (c). On the other hand, T550 surface revealed intergranular (IG) cracking and grain decohesion associated with IGC as shown in Fig. 8 (e)-(h).

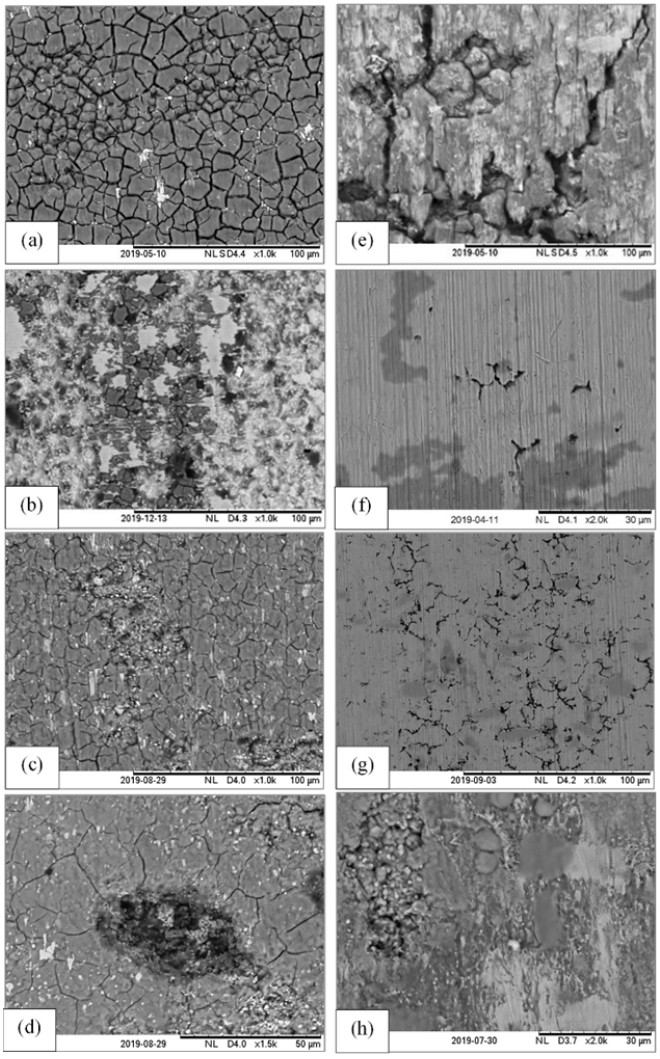


Fig. 8 Microscopic surface morphology of (a), (b) T200-ACSF, (c), (d) T200- deaerated PBS, (e), (f) T550- deaerated ACSF, and (g), (h) T550- deaerated PBS.

### C. Corrosion Products and Passive Films

The EDX results indicated that corrosion products collected from PBS mainly consisted of iron (Fe), oxygen (O) and phosphorus (P), whereas that of ACSF composed of iron (Fe) and oxygen (O). The XRPD results could identify that corrosion product in PBS comprised of vivianite ($Fe_3(PO_4)_2 \cdot 8H_2O$)) mixed with some sodium chloride (NaCl) and Fe, whereas the presence of graphite (C) and goethite (FeO(OH)) were detected in ACSF corrosion product.

Table III presents the atomic ratios of passive films formed on both T200 and T550 rods immersed in PBS and ACSF for 2 months. Based on the composition of 440C SS, the ratio of Fe/Cr is in the range of 4.4-5.5. This ratio is postulated as a representative of fresh surface for comparison. The Cr/O ratio was considered as the original protective film of SS, possibly in the form of chromium oxide ($Cr_2O_3$) [22]. The Fe/O ratio was a representative ratio of iron oxide passive film in multiple forms when SS interacts with solutions [29]-[31]. The initial form of goethite (FeO(OH)) passive film was detected by XRPD. This film is known as a GR film when it reacts with DO in solution [32], [33]. The Fe/P ratio could indicate a GR phosphate film ($GR(PO_4^{3-})$) or Vivianite when SS exposed in buffered-phosphate solutions [29]-[32], whereas the Fe/Cl and Fe/S would identify as a GR chloride ($GR(Cl^-)$) and GR sulphate ($GR(SO_4^{2-})$) film [34].

After immersion test, of both rods, the passive film in the shiny areas mainly consisted of iron (Fe), chromium (Cr) and oxygen (O), with the ratios of Fe/Cr = 3.7-6.1, Fe/O = 2.9-10.0 and Cr/O = 0-2. Comparing with the ratio of the original surface, the shiny areas were considered as the remaining of finishing surface or uncorroded areas. Considering the sensitization effect, the Fe/O and Cr/O ratios on unsensitized T200 rods tended to be higher than the sensitized T550. This could be the result of chromium depletion at the vicinity of GBs causing sensitization of T550 rods in chloride solutions [35].

Comparing with PBS, the Fe/O and Cr/O ratios were likely lower in ACSF as it is more aggressive than PBS. Due to the interaction of anion species and iron oxide films, the presence of P was observed on GR film of T200 in PBS, with the Fe/P ratio of 4.5-16.2, whereas there was no Vivianite formed on T550. In ACSF, the Fe/S ratio of 2.8-11.6 was detected on T200 and 6.9-10.5 for T550. The ratio of Fe/Cl on both T200 and T550 in ACSF and PBS was in the range of 7.7- 27.4. It is noted that a ratio of Fe/P, Fe/Cl and Fe/S > 100 is an error from a trace detection.

### D. Metal Ion Release

Fig. 9 exhibits the concentrations of dissolved Fe, Cr and Ti ions in aerated and deaerated ACSF after 2-month immersion. The concentration of Fe ions in aerated ACSF was 26% higher than deaeration. In both conditions, the Cr ions were released about 90 µg/L. Even though there was no change in mass loss of Ti6Al4V collars, a trace of Ti ions was detected in deaerated ACSF up to to 6 µg/L. It was noted that, in PBS, the ICP-OES was limited to detect the dissolved Fe, Cr and Ti ions.

## IV. Discussion

This study has presented an *in vitro* immersion test design that simulates the construct of the screw driving components in an MCGR operating in the spine. Dissimilar 440C SS-Ti6Al4V couples were used to study the galvanic effect. Also, the *in vivo* environment was modelled by performing the tests in 37 °C ACSF and PBS controlling DO level at 1 and 5 ppm for 2 months. The 440C SS was heat-treated at 200 and 500 °C to produce unsensitized T200 and sensitized T550

microstructures to evaluate probable corrosion resistance *in vivo*. Also, environmental factors affecting CRs and its mechanisms were determined. This study indicates that there are five factors affecting CRs and mechanisms including pH, DO, anion species, microstructures and dissimilar coupling design.

TABLE III
ATOMIC RATIOS OF PASSIVE FILMS ON T200 AND T550 RODS IN PBS AND ACSF

| Rods | Analysed areas | Solutions | Ratio of Fe/Cr | Ratio of Fe/O | Ratio of Cr/O | Ratio of Fe/P | Ratio of Fe/Cl | Ratio of Fe/S |
|---|---|---|---|---|---|---|---|---|
| T200 | Finishing surface (shiny) | PBS | 3.8-6.1 | 3.9-4.8 | 0.8-1.0 | - | - | - |
| | | ACSF | 3.8-4.3 | 0.9-7.2 | 0.2-1.9 | - | 142 | 108 |
| | GR film | PBS | 1.0-1.5 | 0.20 | 0.10 | 4.5-16.2 | 12.4-27.4 | - |
| | | ACSF | 0.6-1.1 | 0.1-0.2 | 0.1-0.2 | - | 7.7-19.0 | 2.8-11.6 |
| T550 | Finishing surface (shiny) | PBS | 5.0-5.5 | 2.9-10.0 | 0.5-2.0 | 105 | - | - |
| | | ACSF | 3.7 | 1.5 | 0.4 | - | 168 | - |
| | Discoloration (matte) | PBS | 4.9 | 4.0 | 0.81 | 155 | 164 | - |
| | | ACSF | 0.6-0.8 | 0.10 | 0.20 | - | 19.4-19.8 | 6.9-10.5 |

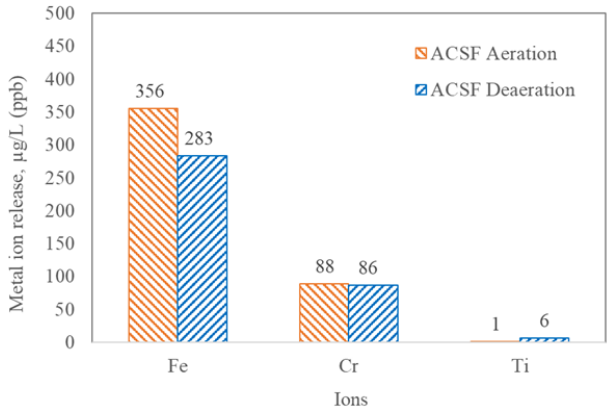


Fig. 9 Concentration of metal ion release in aerated and deaerated ACSF after 2-month immersion

First, pH plays an important role to control chemical reactions in corrosion cells and stability of the passive films [30], [31]. The results of this study show that the pH values of PBS changed from neutral into alkaline (10-11). Conversely, the neutral ACSF had turned into acidic (5.5). Consequently, CR of 440C rods in ACSF is higher than PBS, up to 5 times. Comparing to DI water, it had become little acidic (~6) and the CR of 440C rods is about 5 times lower than that of PBS. However, pH change had not affected the mass loss of Ti6Al4V collars. Similarly, Kovacevic et al. studied the influence of pH on corrosion behavior of 316L and Ti6Al4V implants in Hanks solution. The authors found that the solution became acidic and caused more significant corrosion on SS, comparing with Ti6Al4V [36].

Second, DO affects the stability of the passive films of implant alloys [8]. Raja and Jones [37] found that DO is necessary for re-passivation of 316L in sulfuric acid. However, the increase of DO could cause a decrease in passivation properties of martensitic and austenitic SS [38]-[40]. This is unlike Ti alloys which attribute the stability of passive film in oxidizing media under aeration and deaeration [8]. Considering the present findings, the CR of 440C rods in aerated ACSF is relatively higher than deaerated condition, with 1.8 times for T200 and 3.2 times for T550. Conversely, in PBS, a significant CR increase has been observed under deaeration than aeration, with 1.8 times for T200 and 1.2 times for T550. These results imply that the presence of higher oxygen in ACSF in acidic condition may accelerate the dissolution of GR($SO_4^{2-}$) [41]. On the contrary, less oxygen (deaeration) in PBS promotes CR due to instability of GR($PO_4^{3-}$) passive film [42]. Due to the different anion species between ACSF and PBS, the distinct CR and corrosion behavior of 440C rods depend on passive film properties.

Third, anion species in bulk electrolytes affect the properties of passive films. When iron-based alloys react with aqueous solutions, magnetite ($Fe_3O_4$) is formed [31]. The $Fe_3O_4$ is proportional to hydroxide ($OH^-$) ions at the alkaline condition. The GR(FeO(OH)) film is then produced on SS by the oxidation of magnetite. A decrease of $Fe_3O_4$ film results in acidic condition. Kiyama and Takada [34] indicate that goethite (α-FeO(OH)) was the first form of the GR passive film, followed by akaganeite (β-FeO(OH)) and lepidocrocite (γ-FeO(OH)). This film, then, reacted with anion species in solutions and formed different passive films which attributed the distinct corrosion properties. It has been observed that the GR films formed on the iron-based steels in solutions containing chloride, sulphate, carbonate and phosphate anions, designated as GR($Cl^-$), GR($SO_4^{2-}$), GR($CO_3^{2-}$) and GR($PO_4^{3-}$) respectively [32], [41], [43]. Each GR type had the unique properties which could impede or accelerate CR. Hansen and Poulsen [44] found that GR($PO_4^{3-}$) or vivianite ($Fe_3(P0_4)_2{\cdot}8H_2O$) film which formed in phosphate-containing solutions behaved as a protective film and delayed corrosion. The stability of vivianite increases in phosphate-rich solutions and intensity of GR(FeO(OH)) film relating to high pH (alkaline) and low oxygen (deaeration) [42]. In contradiction to sulphate containing solutions, GR($SO_4^{2-}$) film is precipitated at low pH (acidic condition). This biofilm is active and tends to form microbiologically influenced corrosion if infection proceeds [45]-[47].

In this study, ACSF comprises aggressive chloride and sulphate ions with the $Cl^-/SO_4^{2-}$ ratio of 7.5, whereas PBS contains aggressive chloride and phosphate inhibitor with the $Cl^-/PO_4^{3-}$ ratio of 4.4. The EDX results of corrosion products and passive films show the presence of phosphorus (P) in PBS and sulphur (S) in ACSF. The XRPD results indicate that

vivianite was formed in PBS, whereas graphite and trace of goethite (FeO(OH)) were detected in ACSF. The tendency of CR of T200 and T550 in ACSF is higher than that of PBS, 1.6 – 5.2 times. This could confirm that GR($PO_4^{3-}$) film formed in alkaline PBS has more corrosion resistance than the GR($SO_4^{2-}$) film precipitated in acidic ACSF. However, this tendency has been reversed for the CR of T550 rods in deaerated condition. This is because the formation of GR(FeO(OH)) film is proportional to the DO level as oxygen is used for oxidation of $Fe_3O_4$ [32], resulting in the limitation of vivianite formation. Comparing with DI water, it is supposed that $Fe_3O_4$ passive film formed on 440C rods at pH of 6 and the CR is 5 times lower than PBS. The corrosion resistance of passive films could rank as GR($PO_4^{3-}$) > $Fe_3O_4$ > GR($SO_4^{2-}$).

Fourth, the HT process controls microstructure, mechanical and corrosion properties of heat-treatable alloys. Regarding martensitic SS, chromium is depleted at the GBs if it is tempered at the temperature of 450-600 °C, resulting in the deficiency of pitting corrosion resistance and susceptibility of intergranular (IG) corrosion [23], [24]. Unlike the unsensitized microstructure, it tends to undergo uniform corrosion in the corrosive environment [23]. The present results show that the CR of sensitized T550 rods is relatively higher than the unsensitized T200 in both PBS and DI water. Conversely, in ACSF, it is evident that T550 accounted for more corrosion resistance than T200 rods due to different passivation properties. However, in terms of surface morphology characteristic, IG corrosion poses a high risk of cracking rather than uniform corrosion. If it is combined with mechanical loading, stress corrosion cracking or corrosion fatigue may cause a sudden fracture. As seen from SEM results (Figs. 8 (e)-(h)), T550 underwent carbide decohesion combined with IG cracking. Additionally, the IG crack tends to behave like a stress concentration site, leading to reduction in strength and toughness properties.

Fifth, the dissimilar coupling design affects corrosion mode of 440C rods. According to galvanic series, a Ti acts as a cathode with potential (+0.04 to -0.12 V), whereas a martensitic SS plays as an anode (-0.45 to -0.53 V) [22]. In electrolytes, the anode sacrifices itself as the protection of cathode; as a result, corrosion at the cathode is suppressed. As the cathodic surface area controls CR of the anodic area, corrosion becomes severe if localized pits are formed as the anode area decreases. Regarding the dissimilar 440C SS – Ti6Al4V couples with the cathode/anode ratio of 3.4, the 440C SS rod acting as an anode was corroded up to 480 µm/yr, whereas mass loss of Ti6Al4V collars rarely changed for 2-month immersion. The results of macroscopic surface morphology in Fig. 7 show that the GR film and discoloration were favorably formed on the 440C rod surface at the connection areas with the Ti6Al4V collars. Based on the surface morphology of 440C rods after 1 and 2 months immersion, the evolution of corrosion characteristics is simplified and presented in Fig. 10.

Fig. 10 (a) presents the formation of passive films which formed intensely on the 440C rods at the junction of Ti6Al4V collars (confined areas). This feature could confirm that the initial stage of corrosion process was dominated by the galvanic effect in electrolytes. After 1-month immersion, some pits were selectively developed on the 440C rods between both gaps of Ti6Al4V collars and propagated to the inner side of the confined areas as shown in Fig. 10 (b). This characteristic could indicate a typical feature of crevice corrosion. Due to the variation of cathode/anode ratio, the smaller areas of pits became the anodic areas, whereas the cathodic areas increased by the combination of passive film areas of 440C rod and Ti6Al4V areas. Consequently, corrosion characteristic became more severe by the presence of pits and the increasing CR after 2-month immersion. The dissolution of passive films was also observed in the confined areas as the variation of DO level could affect the stability of passive films. This may affect the tendency of CR as the severity of corrosion depends on the re-passivation and passive film properties of 440C rods.

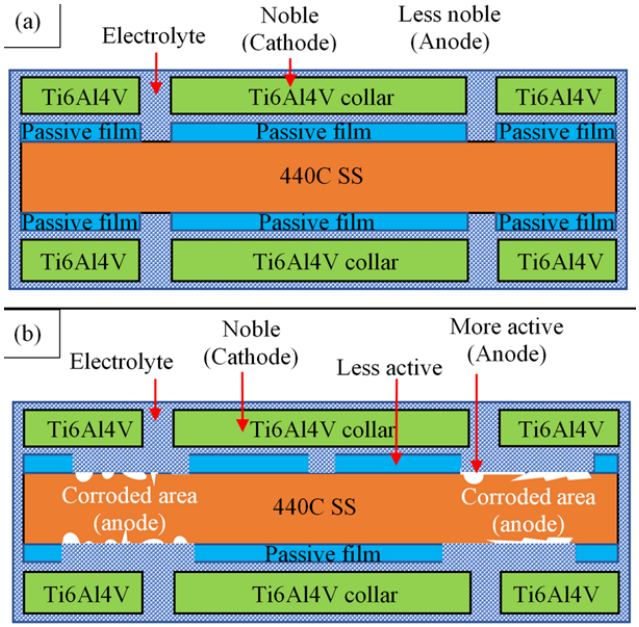


Fig. 10 Schematics of corrosion evolution changing by the surface areas of cathode and anode. (a) stable passive film and (b) pit formation and passive film dissolution

Fig. 11 illustrates the simplified diagrams of pit formation and dissolution of passive films on T200 and T550 rods varying by oxygen concentration cells, based on the macroscopic surface morphology in Fig. 7. On T200 rods in Fig. 11 (a), the macroscopic morphology showed the different shades of GR films in the confined areas induced by differential oxygen concentration. Due to the increase of DO, the dissolution process of passive films would be accelerated [40]. The distinct shade of GR film could indicate the decomposition of passive films which could be confirmed by the microscopic morphology in Figs. 8 (a)-(d) appearing as the mud-cracking pattern and passive film removal. On the other hand, the microscopic characteristic of T550 rods indicated IG corrosion and cracking. These features became severe in the confined areas due to differential oxygen concentration cells

causing crevice corrosion in macroscale, as illustrated in Fig. 11 (b).

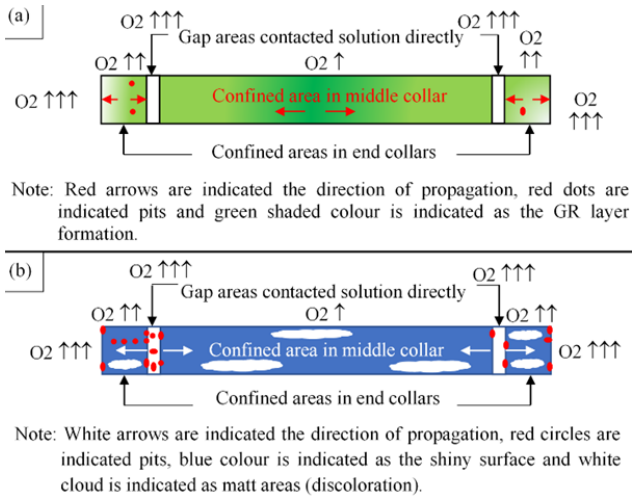


Fig. 11 Schematics of corrosion evolution showing the differential oxygen concentration cells. (a) T200 and (b) T550

In terms of metal ion release, it has been advised that, according to the Medicines and Healthcare Products Regulatory Agency (MHRA), the concentration of whole blood Co and Cr should not exceed than 7 µg/L [48]. If the blood test results are over than the criterion, MRI or ultrasound scans should be assessed to indicate the potential for adverse symptoms of soft tissues. Although there was no corrosion sign on the implants, high levels of nickel (Ni) and chromium (Cr) were detected in both serum and urine after 10-year SS implantation [49]. In the presence of macroscopic corrosion, much higher Cr ions released after 316L SS spinal implantation than the criterion was observed 33 and 97 µg/L in serum and urine, compared to the normal limit of 0.16 and 0.22 µg/L respectively. Moreover, the significant levels of Co, Cr and Ni with the adverse symptoms were also detected at the local tissue of failed hip prosthesis, with 187, 752.6 and 3.99 µg/g, respectively [50]. However, these data are unable to identify the generating sources that possibly resulted from wear debris or corrosion or synergy reactions. Regarding Ti release, Levine et al. also observed that Ti serum hit to 2.9 µg/L after 36-month hip replacement, before gradually dropping to 1.7 µg/L in 108 months [51]. The adverse symptom at the distal tissues such as yellow nail syndrome was also observed after Ti dental implantation [52]. Despite evidently over 95% of Ti serum detection, there is no recommended limit for Ti serum [53]. As there is no sign of implant site infection by Ti, the biological and clinical responses of elevated Ti serum remain unclear. Wisbey et al. [54] stated that Ti ions released from Ti6Al4V implants in 0.17 M NaCl plus 0.0027 M EDTA at 37 °C were less than $2.5x10^{-3}$ µg/cm$^2$/hr or 0.25 µm/yr. In the present work, after 2-month immersion in ACSF, Fe and Cr ions released from 440C SS about 360 and 90 µg/L which is higher than the MHRA criterion. Even though there is no mass loss observed in Ti6Al4V, 6 µg/L of Ti ions dissolved were detected in deaerated ACSF. In terms of CR by surface area, it was about $4.1x10^{-5}$ µg/cm$^2$/hr.

Overall, the use of dissimilar 440C SS-Ti6Al4V couplings in the encapsulated MCGRs is intended for dry use. When the sealing mechanism allows body fluid ingress, corrosion proceeds in the casing. The corrosion resistance of unsensitized 440C SS is better than the sensitized one in PBS and DI water, whereas the sensitized 440C has better resistance in ACSF. As the synergy of corrosive chloride and sulphate ions in ACSF are more aggressive, the balance of corrosive chlorides and phosphate inhibitor in PBS with the ratio of 1:4.4 could minimize CR of 440C SS about 5 times for unsensitized 440C and 2 times for the sensitized. These findings may support the application of phosphate coated surface treatment for metallic implants [55]-[57]. Even though the sensitized 440C SS has better corrosion resistance in the aggressive environment than the unsensitized in terms of mass loss, it poses a high risk of IG cracking when corrosion is combined with stresses.

## V. Conclusion

The screw driving components in an MCGR system operating *in vivo* in the spine were modelled *in vitro* using 440C SS rods and Ti6Al4V collars immersed in 37 °C PBS and ACSF under aeration and deaeration. Three main factors influenced CR and corrosion mechanism of 440C SS are concluded as follows:

1) Environmental factors:
- pH variation: The formation of the passive film in the alkaline condition is more stable than the acidic medium. The CR of 440C SS in alkaline PBS was less than that of acidic ACSF.
- DO level: The stability of passive film varied by DO level. High oxygen in acidic ACSF and low oxygen in alkaline PBS may accelerate CR of 440C SS.
- Anion species: The balance of corrosive chloride ion and phosphate inhibitor in PBS would delay corrosion. On the other hand, the synergy of aggressive chloride and sulphate ions in ACSF would enhance CR of 440C SS.

2) HT factor: the tempering temperature at the critical range of 440C SS led to sensitization in the corrosive environment. In terms of mass loss, the sensitized 440C had better corrosion resistance in ACSF. However, the sensitized 440C SS underwent IG corrosion and cracking. The unsensitized 440C SS without couping tended to be dominated by uniform corrosion due to passive film dissolution.

3) Combination of dissimilar alloys and coupling design: the corrosion process of the unsensitized 440C started by the galvanic effect, appearing as the formation of intense passive film at the confined areas. Then, crevice corrosion was predominated in forms of pits and passive film removal in the confined areas due to the change in differential oxygen concentration cell. Unlike the sensitized 440C, the micro-mechanism was initially driven by IG corrosion and then IG cracking and grain

decohesion were developed between both gaps and the confined areas, appearing as crevice corrosion in macroscale.

The findings from this study suggest that the combination of 440C SS-Ti6Al4V couples in the encapsulated MCGR implants becomes undesirable if they are exposed to high humidity or the corrosive environment *in vivo* due to the synergy of galvanic and crevice effects. The HT at the critical temperature range of 440C SS should be avoided to prevent IG cracking. Life assessment would be helpful to manage the revision plan for replacement. As the risk of metallosis is high, the use of 440C SS-Ti6Al4V couples for invasive application *in vivo* should be carefully designed and followed up. The durability of the sealing mechanism should be also improved to minimize the possibility of corrosion.

## ACKNOWLEDGMENT

The authors would like to thank the staff of Merz Court Analytical Suite and Advanced Chemical and Materials Analysis Units at the School of Engineering, Newcastle University, UK for their ICP-OES, EDX and XRPD support.

## REFERENCES

[1] J. R. Davis, Ed., *Metallic Materials, Handbook of Materials for Medical Devices*. ASM International, 2003.

[2] R. A. Ganz, "A Modern Magnetic Implant for Gastroesophageal Reflux Disease," *Clin Gastroenterol Hepatol*, vol. 15, no. 9, pp. 1326–1337, Sep. 2017.

[3] D. Paley, "PRECICE intramedullary limb lengthening system," *Expert Rev Med Devices*, vol. 12, no. 3, pp. 231–49, 2015.

[4] P. Hosseini *et al.*, "Magnetically controlled Growing Rods for Early-onset Scoliosis: A Multicenter Study of 23 Cases with Minimum 2 years Follow-up," *Spine*, vol. 41, no. 18, pp. 1456–1462, Sep. 2016.

[5] V. C. Panagiotopoulou *et al.*, "Analysing a mechanism of failure in retrieved magnetically controlled spinal rods," *Eur Spine J*, vol. 26, no. 6, pp. 1699–1710, 2017.

[6] K. H. Teoh *et al.*, "Magnetic controlled growing rods for early-onset scoliosis: a 4-year follow-up," *The Spine Journal*, vol. 16, no. 4, Supplement, pp. S34–S39, Apr. 2016.

[7] K. H. Teoh *et al.*, "Metallosis following implantation of magnetically controlled growing rods in the treatment of scoliosis," *Bone Joint J*, vol. 98-B, no. 12, pp. 1662–1667, Dec. 2016.

[8] N. Eliaz, "Corrosion of Metallic Biomaterials: A Review," *Materials (Basel)*, vol. 12, no. 3, Jan. 2019.

[9] S. I. Tafazal and P. J. Sell, "Incidental durotomy in lumbar spine surgery: incidence and management," *Eur Spine J*, vol. 14, no. 3, pp. 287–290, Apr. 2005.

[10] Y. Shiono *et al.*, "Delayed Propionibacterium acnes surgical site infections occur only in the presence of an implant," *Sci Rep*, vol. 6, p. 32758, 12 2016.

[11] R. Khazim *et al.*, "Incidence and treatment of delayed symptoms of CSF leak following lumbar spinal surgery," *Eur Spine J*, vol. 24, no. 9, pp. 2069–2076, Sep. 2015.

[12] T.-Y. Lin *et al.*, "Postoperative meningitis after spinal surgery: a review of 21 cases from 20,178 patients," *BMC Infectious Diseases*, vol. 14, no. 1, p. 220, Apr. 2014.

[13] M. K. Kasliwal, L. A. Tan, and V. C. Traynelis, "Infection with spinal instrumentation: Review of pathogenesis, diagnosis, prevention, and management," *Surg Neurol Int*, vol. 4, no. Suppl 5, pp. S392-403, 2013.

[14] M. E. Portillo, S. Corvec, O. Borens, and A. Trampuz, "Propionibacterium acnes : An Underestimated Pathogen in Implant-Associated Infections," *BioMed Research International*, 2013.

[15] N. u. O. Jeelani, A. V. Kulkarni, P. DeSilva, D. N. P. Thompson, and R. D. Hayward, "Postoperative cerebrospinal fluid wound leakage as a predictor of shunt infection: a prospective analysis of 205 cases: Clinical article," *Journal of Neurosurgery: Pediatrics*, vol. 4, no. 2, pp. 166–169, Aug. 2009.

[16] F. Hahn, R. Zbinden, and K. Min, "Late implant infections caused by Propionibacterium acnes in scoliosis surgery," *Eur Spine J*, vol. 14, no. 8, pp. 783–788, Oct. 2005.

[17] B. Bose, "Delayed infection after instrumented spine surgery: case reports and review of the literature," *Spine J*, vol. 3, no. 5, pp. 394–399, Oct. 2003.

[18] B. R. Richards and K. M. Emara, "Delayed infections after posterior TSRH spinal instrumentation for idiopathic scoliosis: revisited," *Spine*, vol. 26, no. 18, pp. 1990–1996, Sep. 2001.

[19] *ASM Handbook Volume 23: Materials for Medical Devices*. ASM International, 2012.

[20] I. F. Pye and G. M. Aber, "Interrelations between cerebrospinal fluid and plasma inorganic ions and glucose in patients with chronic renal failure.," *J Clin Pathol*, vol. 35, no. 6, pp. 631–637, Jun. 1982.

[21] *ASM Handbook Volume 11: Failure Analysis and Prevention*. ASM International, 2002.

[22] Sedriks, *Corrosion of Stainless Steels 2e*, 2 edition. New York: John Wiley & Sons, 1996.

[23] S. K. Bonagani, V. Kain, and B. Vishwanadh, "Effect of Tempering Treatments on Microstructure and Intergranular Corrosion of 13 wt% Cr Martensitic Stainless Steel," *CORROSION*, vol. 73, no. 4, pp. 362–378, Dec. 2016.

[24] S. K. Bonagani, V. Bathula, and V. Kain, "Influence of tempering treatment on microstructure and pitting corrosion of 13 wt.% Cr martensitic stainless steel," *Corrosion Science*, vol. 131, pp. 340–354, Feb. 2018.

[25] K. C. Zartman, G. C. Berlet, C. F. Hyer, and J. R. Woodard, "Combining dissimilar metals in orthopaedic implants: revisited," *Foot Ankle Spec*, vol. 4, no. 5, pp. 318–323, Oct. 2011.

[26] "ASTM F899 - 12b: Standard Specification for Wrought Stainless Steels for Surgical Instruments." ASTM International, Dec. 2012.

[27] "ASTM F136 - 08 Standard Specification for Wrought Titanium-6 Aluminum-4 Vanadium ELI (Extra Low Interstitial) Alloy for Surgical Implant Applications." ASTM International.

[28] "ASTM G31-72 (Reapproved 2004) Standard Practice for Laboratory Immersion Corrosion Testing of Metals." ASTM International.

[29] C. M. Méndez, R. E. Burgos, F. Bruera, and A. E. Ares, "Passive Films Formed on Stainless Steels in Phosphate Buffer Solution," in *Characterization of Minerals, Metals, and Materials 2016*, Cham: Springer International Publishing, 2016, pp. 563–570.

[30] L. Freire *et al.*, "Electrochemical and analytical investigation of passive films formed on stainless steels in alkaline media," *Cement and Concrete Composites*, vol. 34, no. 9, pp. 1075–1081, Oct. 2012.

[31] L. Freire, M. J. Carmezim, M. G. S. Ferreira, and M. F. Montemor, "The electrochemical behaviour of stainless steel AISI 304 in alkaline solutions with different pH in the presence of chlorides," *Electrochimica Acta*, vol. 56, no. 14, pp. 5280–5289, May 2011.

[32] G. Sahoo, S. Fujieda, K. Shinoda, and S. Suzuki, "Influence of phosphate species on green rust I transformation and local structure and morphology of γ-FeOOH," *Corrosion Science*, vol. 53, no. 8, pp. 2446–2452, Aug. 2011.

[33] L. Wang, K. Daub, Z. Qin, and J. C. Wren, "Effect of dissolved ferrous iron on oxide film formation on carbon steel," *Electrochimica Acta*, vol. 76, pp. 208–217, Aug. 2012.

[34] M. Kiyama and T. Takada, "Iron Compounds Formed by the Aerial Oxidation of Ferrous Salt Solutions," *BCSJ*, vol. 45, no. 6, pp. 1923–1924, Jun. 1972.

[35] S. Lynch, "A review of underlying reasons for intergranular cracking for a variety of failure modes and materials and examples of case histories," *Engineering Failure Analysis*, vol. 100, pp. 329–350, Jun. 2019.

[36] N. Kovačević, B. Pihlar, V. S. Šelih, and I. Milošev, "The Effect of pH Value of a Simulated Physiological Solution on the Corrosion Resistance of Orthopaedic Alloys.," *Acta chimica Slovenica*, vol. 59, no. 1, pp. 144–155, Mar. 2012.

[37] K. S. Raja and D. A. Jones, "Effects of dissolved oxygen on passive behavior of stainless alloys," *Corrosion Science*, vol. 48, no. 7, pp. 1623–1638, Jul. 2006.

[38] X. Yue *et al.*, "Effect of Traces of Dissolved Oxygen on the Passivation Stability of Super 13Cr Stainless Steel Under High CO2/H2S Conditions," *Int. J. Electrochem. Sci.*, pp. 7853–7868, Aug. 2017.

[39] H. Sun, X. Wu, E.-H. Han, and Y. Wei, "Effects of pH and dissolved oxygen on electrochemical behavior and oxide films of 304SS in borated and lithiated high temperature water," *Corrosion Science*, vol. 59, pp. 334–342, Jun. 2012.

[40] G. D. Eyu, G. Will, W. Dekkers, and J. MacLeod, "Effect of Dissolved

Oxygen and Immersion Time on the Corrosion Behaviour of Mild Steel in Bicarbonate/Chloride Solution," *Materials (Basel)*, vol. 9, no. 9, Sep. 2016.

[41] R. Guilbaud, M. L. White, and S. W. Poulton, "Surface charge and growth of sulphate and carbonate green rust in aqueous media," *Geochimica et Cosmochimica Acta*, vol. 108, pp. 141–153, May 2013.

[42] Y. Mao, A. N. Pham, A. L. Rose, and T. D. Waite, "Influence of phosphate on the oxidation kinetics of nanomolar Fe(II) in aqueous solution at circumneutral pH," *Geochimica et Cosmochimica Acta*, vol. 75, no. 16, pp. 4601–4610, Aug. 2011.

[43] G. Ona-Nguema, M. Abdelmoula, F. Jorand, O. Benali, J.-C. Block, and J.-M. R. Génin, "Iron(II,III) Hydroxycarbonate Green Rust Formation and Stabilization from Lepidocrocite Bioreduction," *Environ. Sci. Technol.*, vol. 36, no. 1, pp. 16–20, Jan. 2002.

[44] H. C. B. Hansen and I. F. Poulsen, "Interaction of Synthetic Sulphate 'Green Rust' with Phosphate and the Crystallization of Vivianite," *Clays and Clay Minerals*, vol. 47, no. 3, pp. 312–318, 1999.

[45] M. K. Khouzani, A. Bahrami, A. Hosseini-Abari, M. Khandouzi, and P. Taheri, "Microbiologically Influenced Corrosion of a Pipeline in a Petrochemical Plant," *Metals*, vol. 9, no. 4, p. 459, Apr. 2019.

[46] M. a. Pacha-Olivenza, M. c. García-Alonso, R. Tejero, M. l. Escudero, A. m. Gallardo Moreno, and M. l. González-Martín, "Microbiologically induced corrosion of titanium implants," *Orthopaedic Proceedings*, vol. 99-B, no. SUPP_1, pp. 22–22, Jan. 2017.

[47] I. B. Beech, J. A. Sunner, C. R. Arciola, and P. Cristiani, "Microbially-influenced corrosion: damage to prostheses, delight for bacteria," *Int J Artif Organs*, vol. 29, no. 4, pp. 443–452, Apr. 2006.

[48] "Medicines and Healthcare Products Regulatory agency (MHRA). Medical device alert: All metal-on-metal (MoM) hip replacements (MDA/2012/036).," *GOV.UK*. http://www.mhra.gov.uk/ (accessed Jan. 02, 2020).

[49] "Biological Responses to Metal Implants," FDA U.S. Food & Drug Adminitration, Sep. 2019. (Online). Available: www.fda.gov.

[50] C. H. Lohmann *et al.*, "Periprosthetic Tissue Metal Content but Not Serum Metal Content Predicts the Type of Tissue Response in Failed Small-Diameter Metal-on-Metal Total Hip Arthroplasties," *The Journal of Bone and Joint Surgery-American Volume*, vol. 95, no. 17, pp. 1561–1568, Sep. 2013.

[51] B. R. Levine *et al.*, "Ten-year outcome of serum metal ion levels after primary total hip arthroplasty: a concise follow-up of a previous report*," *J Bone Joint Surg Am*, vol. 95, no. 6, pp. 512–518, Mar. 2013.

[52] K. T. Kim, M. Y. Eo, T. T. H. Nguyen, and S. M. Kim, "General review of titanium toxicity," *Int J Implant Dent*, vol. 5, no. 1, p. 10, Mar. 2019.

[53] T. P. Cundy, W. J. Cundy, G. Antoniou, L. M. Sutherland, B. J. C. Freeman, and P. J. Cundy, "Serum titanium, niobium and aluminium levels two years following instrumented spinal fusion in children: does implant surface area predict serum metal ion levels?," *Eur Spine J*, vol. 23, no. 11, pp. 2393–2400, Nov. 2014.

[54] A. Wisbey, P. J. Gregson, and L. M. Peter, "Effect of surface treatment on the dissolution of titanium-based implant materials," *Biomaterials*, vol. 12, no. 5, pp. 470–473, Jul. 1991.

[55] R. B. Heimann, "Osseoconductive and Corrosion-Inhibiting Plasma-Sprayed Calcium Phosphate Coatings for Metallic Medical Implants," *Metals*, vol. 7, no. 11, p. 468, Nov. 2017.

[56] M. B. Sedelnikova, E. G. Komarova, Yu. P. Sharkeev, T. V. Tolkacheva, I. A. Khlusov, and V. V. Sheikin, "Bioactive calcium phosphate coatings on metallic implants," *AIP Conference Proceedings*, vol. 1882, no. 1, p. 020062, Sep. 2017.

[57] S. Overgaard, "Calcium phosphate coatings for fixation of bone implants. Evaluated mechanically and histologically by stereological methods," *Acta Orthopaedica Scandinavica*, vol. 71, no. sup297, pp. 1–74, Jan. 2001.